JOURNAL OF SOLID STATE CHEMISTRY 119, 349–358 (1995)

Transformation of $VOHPO_4 \cdot 1/2H_2O$ to $(VO)_2P_2O_7$: Crystallographic, Microstructural, and Mechanistic Aspects

C. C. Torardi,* Z. G. Li,* and H. S. Horowitz†

*DuPont Company, *Central Research and Development and †Specialty Chemicals, Experimental Station, Wilmington, Delaware 19880-0356*

and

W. Liang and M.-H. Whangbo

Department of Chemistry, North Carolina State University, Raleigh, North Carolina 27695-8204

Received February 13, 1995; in revised form May 30, 1995; accepted June 8, 1995

A detailed study of the transformation of the butane oxidation catalyst precursor $VOHPO_4 \cdot 1/2H_2O$ to γ-$(VO)_2P_2O_7$ is reported. The vanadyl hydrogen phosphate precursors used in this study were in the form of single crystals and powders, each prepared from aqueous media. Electron microscopy and X-ray diffraction clearly show the transformation to be topotactic: single crystals are converted to pseudomorphs which are unchanged in size or shape with respect to the starting crystals. The pseudomorphs are made up of highly-oriented vanadyl pyrophosphate microcrystals. A large contraction of the atomic structure in the direction perpendicular to the basal plane induces cracks and voids within the crystal. A transformation mechanism involving phosphorus-atom inversion, along with supporting MNDO SCF-MO calculations, is presented. This mechanism accounts for at least some of the interlayer, crystallographic disorder that is often attributed to the sterically hindering effects of residual organics. The generation of cracks to accommodate unit cell shrinkage along the thin dimension of the crystal plates creates additional basal plane surface area that may be beneficial in terms of catalytic performance. © 1995 Academic Press, Inc.

INTRODUCTION

1. Phase Transformation of Vanadyl Hydrogen Phosphate to Vanadyl Pyrophosphate

The transformation of $VOHPO_4 \cdot 1/2H_2O$ to $(VO)_2P_2O_7$, known for its ability to selectively catalyze the oxidation of *n*-butane to maleic anhydride, has been the subject of several studies (1–4). The precursor phase is layered while the vanadyl pyrophosphate, which results from the heating and "dehydration" of that precursor, is three-dimensionally bonded. The structural relationships, on both the atomic and microcrystalline scales, between these two phases have been discussed in the recent literature. On an atomic level, there clearly exists a strong structural relationship as evidenced by single-crystal X-ray diffraction analyses (5–8). A structural association also exists on a larger scale, as noted by Bordes *et al.* (2) in their description of a pseudomorphic relationship between $VOHPO_4 \cdot 1/2H_2O$ and γ-$(VO)_2P_2O_7$ based on scanning and transmission electron microscopy and electron diffraction results.

Bordes *et al.* (2) and Torardi and Calabrese (6) proposed simple structural conversion mechanisms in which all framework V–O and P–O bonds remain intact, but weak vanadium–water and phosphorus–water bonds are broken. In the mechanism of Torardi and Calabrese (6), the hydrogen phosphate groups condense into pyrophosphate moieties through an inversion of the phosphorus centers without bulk atomic diffusion or sliding of the precursor's layers. A recent time-resolved powder neutron diffraction study of $VOHPO_4 \cdot 1/2H_2O$ by Amorós *et al.* (4) led to results consistent with this phosphorus inversion mechanism. However, Amorós *et al.*, in the belief that the hydrogen–phosphate groups are inadequately oriented to condense into pyrophosphate entities, interpreted their results in favor of a mechanism involving atomic diffusion. This interpretation may have resulted from an incomplete understanding of the inversion mechanism as originally proposed. In the present work, we present a detailed description of this mechanism, along with supporting energy calculations and experimental results including electron microscopy, X-ray and electron diffraction, and surface area data. Our study expands upon the previous work of Bordes *et al.* (2) to further clarify the nature of this phase transformation.

Perhaps the most well known characteristic of the vanadyl hydrogen phosphate to vanadyl pyrophosphate trans-

0022-4596/95 $12.00

TABLE 1
Unit Cell Relationships between $VOHPO_4 \cdot 1/2H_2O$ and $(VO)_2P_2O_7$[a]

	a (Å)	b (Å)	c (Å)	V (Å^3)
$VOHPO_4 \cdot 1/2H_2O$	7.416	9.592	5.689	404.7
$(VO)_2P_2O_7$	16.594 (8.297 × 2)	9.588	7.735 (3.868 × 2)	1230.6 (307.65 × 4)
Δ	+0.88	0.00	−1.82	−97.0
% change	+11.9	0.0	−32.0	−24.0

[a] References (6) and (8), respectively.

formation is the preservation of the distinctive platelike morphology characterizing the hydrated precursor phase. On the basis of this preservation of morphology, most who have studied this transformation have concluded that it should be characterized as topotactic (1–3, 6, 9, 10). There is not unanimity on this point, however, and for reasons either of energetics (4) or of symmetry (11), it has been claimed that topotaxy cannot be invoked in the description of this transformation. In their review of topotactic reactions, Dent Glasser *et al.* (12) acknowledge that there exists a range of definitions, from quite narrow to rather inclusive, and, consequently, opinions often differ as to whether a particular reaction is topotactic. We choose to adopt the definition favored by Dent Glasser which describes topotaxy as the conversion of a single-crystal starting material into a pseudomorph containing one or more products. Furthermore, these products must occur in a definite crystallographic orientation, exhibiting some three-dimensional structural similarity with the starting material. This appears to be the same definition used by Bordes *et al.* (2) and does not require consideration of transformation mechanism, crystallographic properties of intermediate phases, or symmetry of reactant versus product.

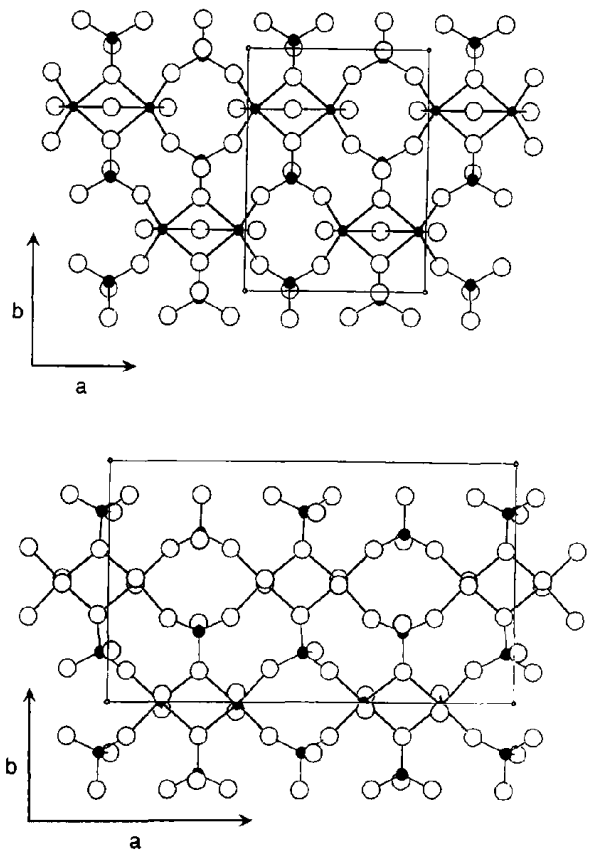

FIG. 1. Structures of: (top) $VOHPO_4 \cdot 1/2H_2O$ viewed down the *c* axis and showing a layer composed of pairs of face-sharing vanadium–oxygen octahedra interconnected by hydrogen–phosphate tetrahedra (see text for more detail). V and P atoms are shaded. (bottom) $(VO)_2P_2O_7$ viewed down the *c* axis and showing pairs of edge-sharing vanadium–oxygen octahedra interconnected by pyrophosphate groups (see text for more detail). V and P atoms are shaded. Some V atoms are obscured by their apical O atoms.

2. *Structural Descriptions*

Crystallographic conventions. Different crystallographic orientations of the orthorhombic $(VO)_2P_2O_7$ unit cell directions have been used in the literature. To discuss and reinforce the structural similarities between $VOHPO_4 \cdot 1/2H_2O$ and $(VO)_2P_2O_7$, we define the basal plane as (001) for both compounds. The convention used in this paper is given in Fig. 1 and Table 1 and is described as follows.

In the precursor, the *c* axis is oriented perpendicular to the layers. In the pyrophosphate, the *c* axis is along the direction of the infinite double strings of O–V ··· O bonds of the *trans* corner-sharing octahedra. The *a* axis is oriented parallel to the V–V vector of the two face-sharing octahedra in the precursor, and essentially parallel to the V–V vector of the two edge-sharing octahedra in the pyrophosphate (Fig. 1).

Stereochemistry of $VOHPO_4 \cdot 1/2H_2O$. The crystal structure of $VOHPO_4 \cdot 1/2H_2O$ (6, 7) consists of vanadyl hydrogen phosphate layers stacked along the *c* axis and held together by interlayer hydrogen bonding. Figure 1a is a view down the *c* axis of the precursor and perpendicular to the layers. Indvidual layers contain pairs of face-sharing VO_6 octahedra. One of the face-sharing oxygen atoms

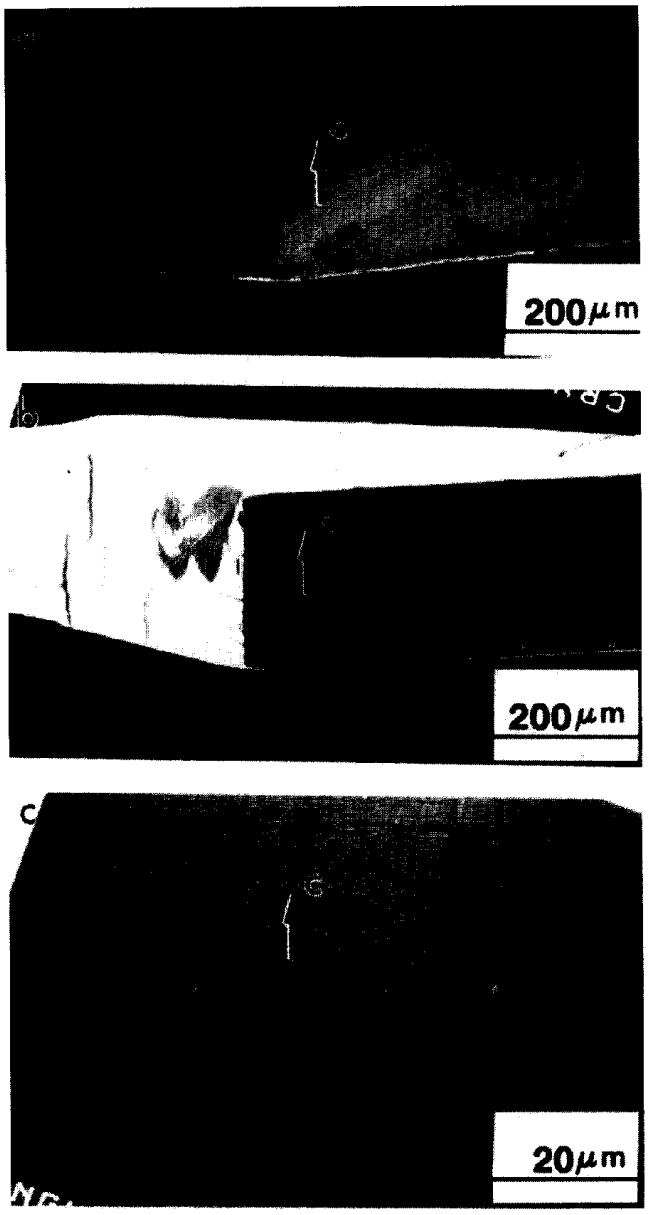

FIG. 2. SEM images of a VPO crystal before (a) and after (b) phase transformation from $VOHPO_4 \cdot 1/2H_2O$. The transformed crystal is shown at higher magnification in (c).

belongs to an H_2O molecule, which bridges the two vanadium atoms and is located *trans* to the vanadyl (V=O) oxygen atoms. The four remaining oxygen atoms of each octahedron are corner-sharing with the base of the O_3POH tetrahedra. Each tetrahedron is oriented with a pseudo threefold axis perpendicular to the plane of the layers, and only the three basal oxygen atoms are shared with vanadium. Hydrogen atoms are bound to the apical oxygen atom of the phosphate groups. Because layers stack directly on top of one another, the O_3POH tetrahedra form strings along the c direction with all the OH units in any given string pointing in the same direction (i.e., either all in the $+c$ direction or all in the $-c$ direction).

Stereochemistry of $(VO)_2P_2O_7$. The pyrophosphate, $(VO)_2P_2O_7$, has a structure (5, 8) related to the precursor, as is illustrated in Fig. 1b, but is covalently bonded in three dimensions. Pairs of edge-sharing VO_6 octahedra are connected along c to form double chains of VO_6 octahedra sharing opposite oxygen corners (see Fig. 8e). Along these chains, the V–O bonds alternate with short–long distances, 1.60 and 2.30 Å. Within the edge-shared octahedral pairs, the vanadyl bonds are oriented in an up–down arrangement (in the c direction). Pyrophosphate groups link the double chains into a three-dimensional network by sharing oxygen corners with vanadium.

EXPERIMENTAL

Single crystals and powders of $VOHPO_4 \cdot 1/2H_2O$, each prepared from aqueous media, were used for the experiments reported here. In this way, complicating effects in the phase transformation due to residual organic molecules in the precursor phase were avoided. In order to study the transformation without interference from competitive oxidation reactions, all transformations were carried out in an inert atmosphere.

Large crystals of the precursor, $VOHPO_4 \cdot 1/2H_2O$, with dimensions up to 3 mm were grown hydrothermally in a sealed gold tube (1.25-cm diameter, 15-cm length) under 3-kbar pressure by heating a mixture of 1.05 g VO_2, 0.28 g V_2O_3, and 8 ml of 3 M H_3PO_4 at 500°C for 12 hr then slowly cooling at a rate of 25°C/hr.

Polycrystalline vanadyl hydrogen phosphate was precipitated out of an aqueous synthesis medium using a procedure adapted from Centi *et al.* (10). V_2O_5 (20 g) was added to 37% HCl (160 g) in a 500 ml round-bottom flask equipped with a mechanical stirrer and reflux condenser. The reaction mixture was heated to reflux under a blanket of nitrogen. Once at reflux temperature, 1.4 g of oxalic acid was added to the reaction vessel followed by the slow addition of 27.4 g of 85% H_3PO_4. After refluxing the black solution for 2 hr, the condenser was removed and replaced by a distillation head. The solution was concentrated, by distillation, to about 40 cc of a very viscous solution. Upon the addition of 50 cc of distilled water the black solution turned dark blue. This solution was then heated to dryness in a vacuum oven. The resulting solid was ground and then stirred for 30 min in boiling water. The washed powder was separated by vacuum filtration and dried in a vacuum at 100°C for 16 hr. This procedure yielded 23.3 g of blue powder. This was shown to be clean $VOHPO_4 \cdot 1/2H_2O$ from X-ray powder diffraction data.

Phase transformations of the single crystal and polycrystalline vanadyl hydrogen phosphates were carried out under flowing nitrogen at either 500 or 700°C. Surface areas

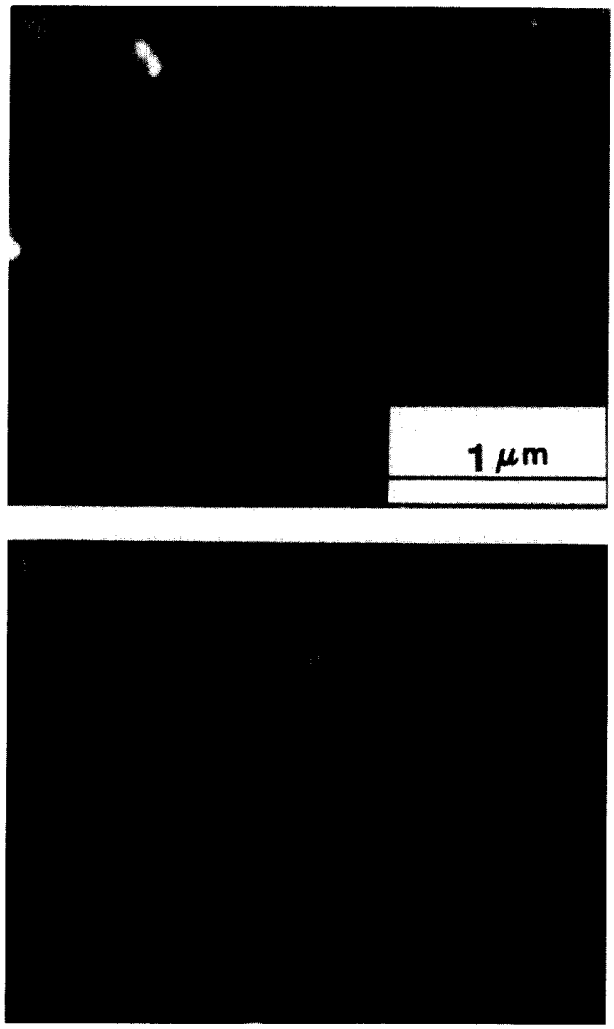

FIG. 3. High magnification SEM of the (001) surface of the VPO crystal before (a) and after (b) phase transformation from $VOHPO_4 \cdot 1/2H_2O$.

of the polycrystalline vanadyl phosphates, both before and after transformation, were measured by nitrogen adsorption using a Micromeritics Model ASAP 2400 instrument. Surface areas were calculated from the nitrogen adsorption isotherm at 77 K using the BET equation (13). In the case of those experiments conducted with single crystal starting material, the transparent blue $VOHPO_4 \cdot 1/2H_2O$ crystals were converted to opaque dark green $(VO)_2P_2O_7$ pseudomorphs by heating at 3–50°C/hr to 500 or 700°C, holding for 12–48 hr, and then cooling at 10–50°C/hr to 150°C. Powder X-ray diffraction on crushed product, using a Scintag PAD V automated powder diffractometer with Cu$K\alpha$ radiation, confirmed transformation to $(VO)_2P_2O_7$. Transformed $(VO)_2P_2O_7$ pseudomorphic "crystals" were also examined on a CAD4 four-circle automated single-crystal X-ray diffractometer with Mo$K\alpha$ radiation, and on a Buerger precession camera with Zr-filtered Mo radiation.

Additional crystallographic characterization was obtained from selected area electron diffraction of both starting and transformed crystals. Microstructural and morphological changes associated with the phase transformation were studied at scales ranging from the mm to the nm range using scanning electron microscopy (JEM 35 and Hitachi S-4000 equipped with a field emission gun) and transmission electron microscopy (JEM 2000FX).

RESULTS

Transformed crystals on the order of 1–3 mm in the plate direction and 0.05–0.5-mm thick, examined by optical

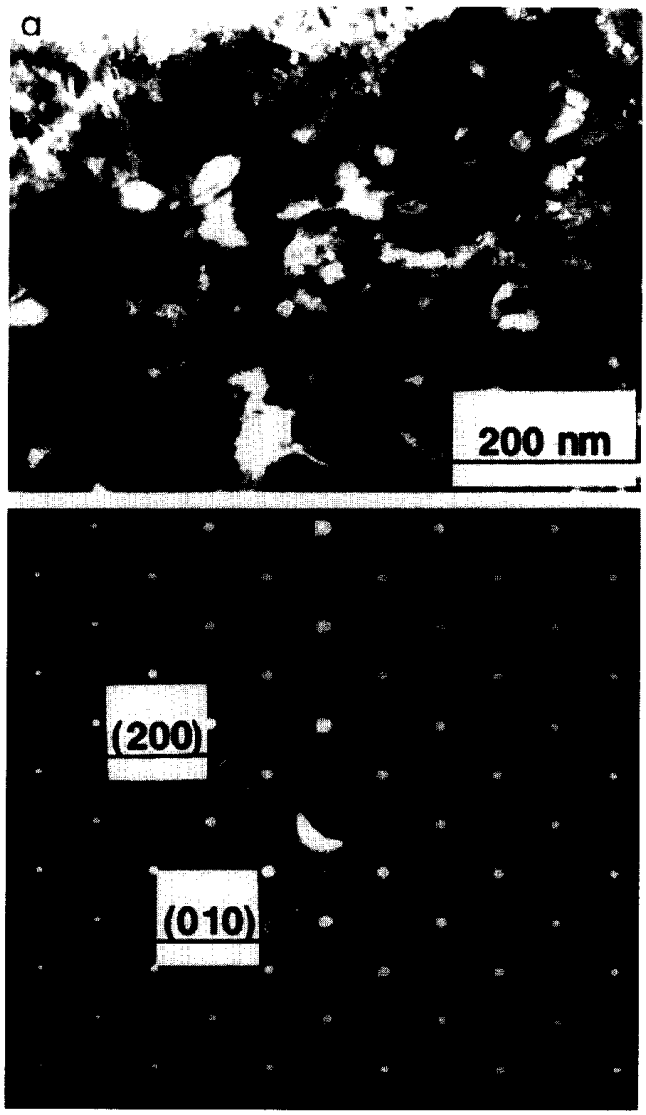

FIG. 4. TEM image (a) and selected area diffraction (SAED) pattern (b) of the $(VO)_2P_2O_7$ pseudomorph after transformation from the $VOHPO_4 \cdot 1/2H_2O$ single crystal. Electron beam oriented perpendicular to (001).

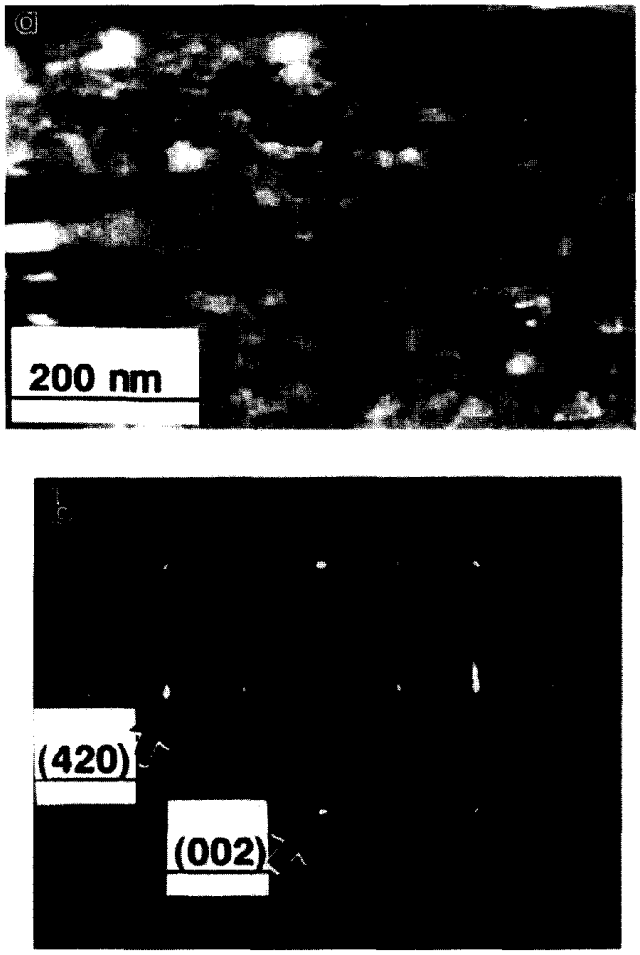

FIG. 5. TEM image (a) and SAED pattern (b) of a $(VO)_2P_2O_7$ pseudomorph after transformation from the $VOHPO_4 \cdot 1/2H_2O$ single crystal. Electron beam oriented parallel to (001).

and electron microscopy, showed very little or no change in their macroscopic dimensions after conversion to the pyrophosphate. Although the starting precursor crystals were single, the pseudomorphs were composed of many small crystals (i.e., microcrystals), as well as microcracks and voids. Figure 2a is an SEM showing the corner of a precursor crystal plate with the *c* axis indicated. Figure 2b shows the same corner of the resulting pseudomorph after transformation at 500°C. The shape of the crystal has not changed and measurement of crystal dimensions before and after transformation confirmed that the size also was not altered. At a higher magnification (Fig. 2c) it is observed that the transformed crystal contains many cracks, most running parallel to the plate surface. Thicknesses of these cracks ranged from less than 0.1 to about 1 μm.

The surface of a precursor single crystal is quite featureless, as seen by the SEM in Fig. 3a. After transformation to the vanadyl pyrophosphate at 500°C under nitrogen, the appearance of this surface is somewhat rough. However, as shown in Fig. 3b, if the transformation is carried out at somewhat higher temperatures (e.g., 700°C), we observe that the surface is much rougher in appearance and is characterized by crystallites which are about 1 μm or less in size, as well as the presence of voids.

Figure 4 shows the TEM image and the selected area diffraction pattern (SAED) of the $(VO)_2P_2O_7$ pseudomorph after heating at 700°C. The electron beam was directed along [001], perpendicular to the "basal plane." Considering the voids observed in the SEM images, we believe that most of the bright regions in the TEM image are due to voids. Some of the light areas in the image are attributed to contrast variations associated with slight misalignments of microcrystals. The SAED pattern shows that all reflections imaged in this orientation (i.e., reflections of crystallographic planes orthogonal to (001)) are fairly sharp.

Figure 5 shows a TEM image and SAED pattern of a similar $(VO)_2P_2O_7$ pseudomorph with the electron beam directed parallel to the plate surface. Variations in contrast in the TEM image clearly show the microcrystalline nature of this pseudomorph, with microcrystals in slightly different orientations giving rise to the mottled appearance. Some of the brighter areas are again due to voids generated during the phase transformation. Figure 6 is a higher resolution image of one of these voids.

High resolution TEM images of the $(VO)_2P_2O_7$ pseudomorphs discussed above in Figs. 4 and 5 are shown in Fig. 7. It illustrates that while the starting single crystals were converted to microcrystalline pseudomorphs, the atomic periodicity is still high within each constituent crystal when viewed both perpendicular and parallel to (001), Figs. 7a and 7b, respectively.

$(VO)_2P_2O_7$ pseudomorphic "crystals" produced patterns on both the single-crystal X-ray diffractometer and the Buerger precession camera which showed fairly sharp diffraction peaks when the crystal was oriented with the *ab* plane perpendicular to the X-ray beam. In fact, several of these *hk*0 level reflections could be found and centered on the automated diffractometer, indicating the high de-

FIG. 6. TEM of a void, formed as a consequence of the topotactic phase transformation, in the $(VO)_2P_2O_7$ pseudomorph.

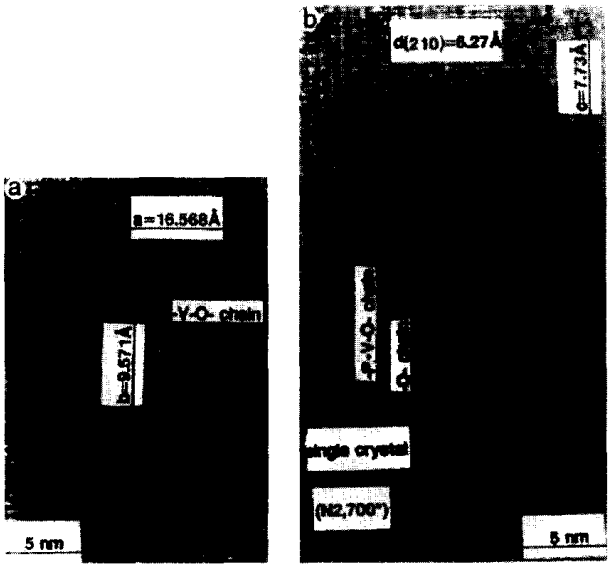

FIG. 7. High resolution TEM of the $(VO)_2P_2O_7$ pseudomorph with the electron beam (a) perpendicular to the (001) basal planes, and (b) parallel with the (001) basal planes.

gree of crystallographic order present in this orientation of the pseudomorphic crystal. As the crystal was tilted away from this orientation, relative to the X-ray beam, the diffraction spots become increasingly broad. Because of this it was not possible to index the pseudomorphic crystal on the automated diffractometer.

DISCUSSION

On an atomic level, very significant changes in the unit cell dimensions accompany the phase transformation from vanadyl hydrogen phosphate to vanadyl pyrophosphate. As the precursor loses its water and OH groups, and the layers condense into the three-dimensional pyrophosphate structure, there occurs a 32% reduction in the unit cell *c*-axis length. In addition, a sizeable expansion (12%) of the *a* axis occurs. The microstructure of the resulting pseudomorph is a consequence of the breaking up of the single crystal precursor into many small crystals of the pyrophosphate, with essentially no change in the crystal's macroscopic dimensions. Evidence for the formation of these microcrystals is found both in the development of observable crystallites on the basal plane surface (see the SEM of Fig. 3b) and the variation in contrast of the TEM images (Figs. 4a and 5a), indicating crystals of slightly different orientations.

Accommodating the considerable unit cell dimension changes while keeping the macroscopic dimensions unchanged is accomplished in two ways. Since expansion of the atomic structure along *a* cannot occur throughout the entire length of the crystal, the microcrystals that are formed are slightly buckled, relative to one another, in and out of the *ab* plane. The large contraction of the atomic structure along *c* causes cracks and voids within the crystal, allowing the macroscopic thickness of the pseudomorph to remain unchanged. Certainly some of the internal porosity created is a simple consequence of the escape of steam when the crystal dehydrates, as discussed by Bordes *et al.* (2). The generation of voids and cracks is not limited to macroscopically large crystals and is also manifested by a change in surface area. As evidence of this, the aqueous-derived polycrystalline $VOHPO_4 \cdot 1/2H_2O$ powder was converted to single phase $(VO)_2P_2O_7$ by heating at 500°C under nitrogen for 16 hr. Surface areas of the precursor and the transformed product were 3 and 12 m^2/g, respectively. As noted previously, a significant portion of the newly created surface area is "basal plane" surface, accompanying the cracks which form parallel to that crystallographic plane. It has previously been suggested (14–16) that the basal plane (i.e., (001) in our notation) represents the catalytically selective surface of the vanadyl pyrophosphate. Thus, formation of these cracks and the accompanying creation of surface area may be beneficial for catalytic performance.

The single-crystal diffractometer and Buerger precession camera results, consistent with the electron diffraction work, indicate that the vanadyl pyrophosphate pseudomorph is derived from relatively well-ordered microcrystals that are highly oriented with respect to one another within the basal (*ab*) planes. While intercrystallite alignment is largely maintained in the basal plane, a slightly greater degree of intercrystallite misalignment is introduced along the *c*-axis direction as a consequence of the phase transformation. The orientation of the pyrophosphate microcrystals is such that the orthorhombic unit cell axial directions essentially coincide with the unit cell axes of the starting orthorhombic, precursor, single crystal.

The experimental results which have just been discussed are highly consistent with the proposed topotactic phosphorus-inverson mechanism (6) for conversion of the $VOHPO_4 \cdot 1/2H_2O$ precursor to the pyrophosphate, $(VO)_2P_2O_7$. A schematic illustration of this mechanism is shown in Figs. 8a–8e. In Fig. 8a, only a small section of two adjacent layers in the precursor is shown. Layers are oriented horizontally in the figure. Pairs of face-sharing VO_6 octahedra in one layer stack directly above the pairs in the neighboring layer. One of the face-shared oxygen atoms in the octahedral pairs belongs to an H_2O molecule, as indicated in Fig. 8a. Note that the V atom forms its short, vanadyl bond with the oxygen atom *trans* to the H_2O oxygen atom. The interconnecting PO_3OH tetrahedra stack directly on top of one another to form strings along the *c*-axial direction with all the OH units in any given string pointing in the same direction (i.e., either all in the

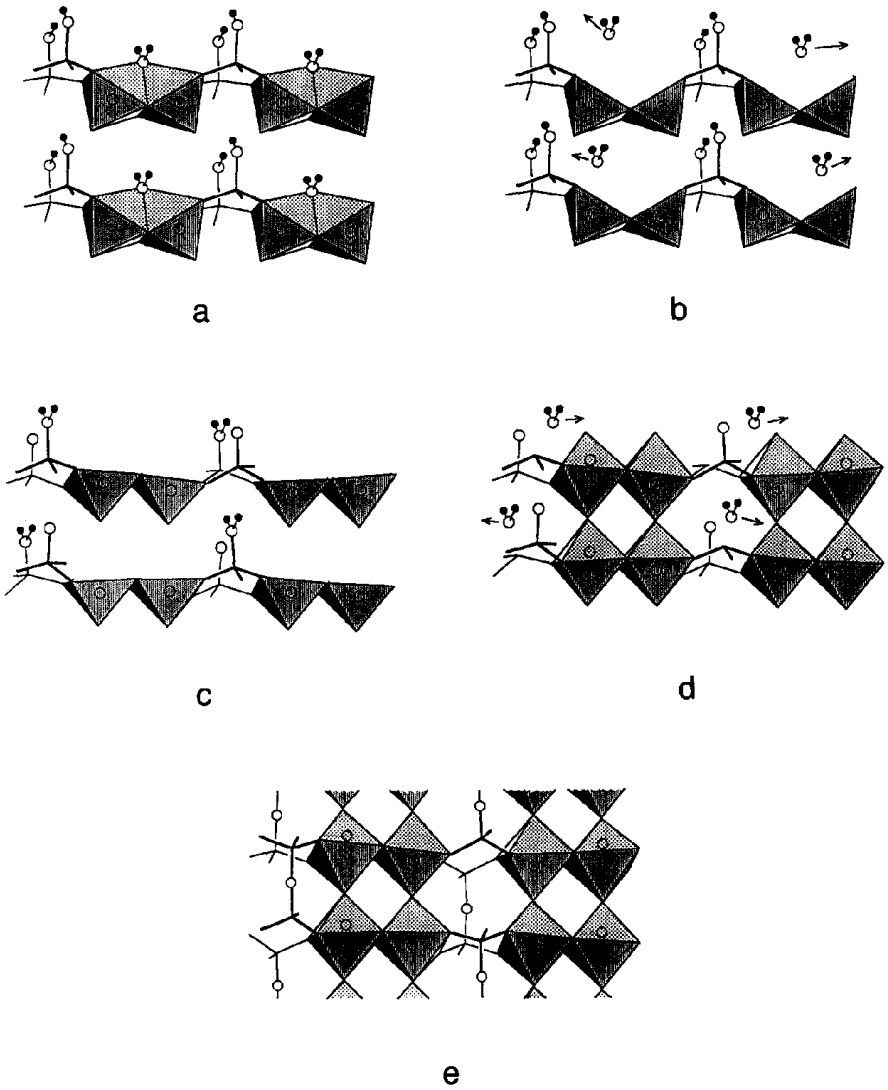

FIG. 8. Illustration of the topotactic phosphorus-inversion transformation mechanism for conversion of the catalysis precursor $VOHPO_4 \cdot 1/2H_2O$ to $(VO)_2P_2O_7$. See text for details.

$+c$ direction or all in the $-c$ direction). Each vanadium pair is surrounded by six PO_3OH groups, four pointing in one direction and two pointing in the opposite direction. For clarity, however, not all of the phosphorous tetrahedra are shown in Fig. 8.

Figure 8b illustrates the loss of the bonded H_2O molecules from the vanadium atom pairs to form edge-shared VO_5 groups and a resultant decrease in the interlayer spacing. Next, the VO_5 pairs pivot about the shared edge to an arrangement where all V=O bonds are approximately parallel (Fig. 8c). This motion expands the layers in the *a*-axial direction and accounts for the 12% increase in the *a*-lattice parameter. Figure 8c also shows half of the O_3POH hydrogens (i.e., protons) transferred to other O_3POH groups to create formally $[O_3P{-}O]^{3-}$ and $[O_3P{-}OH_2]^{1-}$ units. The pathways taken by these protons are not known; however, diffusion of protons, within their respective interlayer regions, to nearby PO_3OH groups is likely. The loss of H_2O molecules from the latter units, leaving behind formally $[O_3P]^{1-}$, is depicted in Fig. 8d. Removal of H_2O allows the layers to fully condense into a three-dimensional network structure. The square-pyramidal VO_5 pairs of one layer connect with those of an adjacent layer by the displacement in the *c* direction of one of the V atoms in a pair toward an apical oxygen atom in the next layer. This creates *trans* corner-sharing VO_6 octahedra with a short–long V–O bond arrangement along any given string of V atoms in the *c* direction and an up–down orientation of the vanadyl bonds within a pair of edge-sharing octahedra; see Fig. 8d. It is easy to see how this up–down orientation

of newly created vanadyl bonds can occur randomly from one double vanadium–oxygen chain to another double chain. Such vanadium-site disorder in vanadyl pyrophosphate crystals grown at high temperature has been discussed by Thompson *et al.* (11).

The highly reactive, coordinately unsaturated $[O_3P]^{1-}$ units can easily invert by movement of the P atom in the *c* direction through the plane of the three basal oxygen atoms to bond to a $[O_3P–O]^{3-}$ unit located above or below the original layer. Figure 8e shows the final interconnected structure of the pyrophosphate. A disorder of the newly created P_2O_7 groups can occur depending on which P atoms invert. At higher temperatures, the pyrophosphate groups rearrange, by breaking and reforming pyrophosphate P–O–P linkages via inversion, into the observed (5, 8), ordered three-dimensional arrangement. Crystallization into the final vanadium- and phosphorus-ordered structure may account for the exothermic peaks observed (2) above 500°C in DTA analyses of the precursor.

It has been suggested (4) that a displacement of the layers of the precursor along the [110] direction would collapse the HPO_4 groups into P_2O_7 units. However, a careful look at the structures of the precursor and pyrophosphate (Figs. 1a and 1b) reveals that although a [110] layer displacement would give proper alignment to form P_2O_7 groups, these groups would have an ordered arrangement different from that actually found in $(VO)_2P_2O_7$ (5, 8). The P_2O_7 arrangement could, of course, convert into the observed arrangement by breaking some P–O–P bonds and inverting the P atoms to bond on the opposite side of the layer. However, such a sliding mechanism followed by an inversion mechanism would require a highly synchronous motion of adjacent layers, which can be easily blocked by the presence of defects. To avoid this difficulty and explain their observation of amorphous intermediates, Amorós *et al.* (4) suggested the involvement of atomic diffusion. However, the latter is unlikely because it will require a high activation energy (of bond breaking). In addition, the amorphous intermediates observed by Amorós *et al.* are consistent with the phosphorus inversion mechanism of Torardi and Calabrese (6).

The degradation of crystallinity or the appearance of an amorphous intermediate is not surprising since significant disruption of the $VOHPO_4 \cdot 1/2H_2O$ structure results in the temperature range where conversion to the pyrophosphate takes place: Water from the face-sharing pairs of vanadium octahedra is evolved, the octahedra move in the *ac* plane to form edge-sharing units, the layers move through a significant distance to link together, additional water from the P–OH groups is ejected, and P atoms randomly link into pyrophosphate groups. In this conversion temperature range, the atoms are "moving", and long-range crystallographic disorder can develop, as described by the model presented here. This is often reflected in the X-ray powder

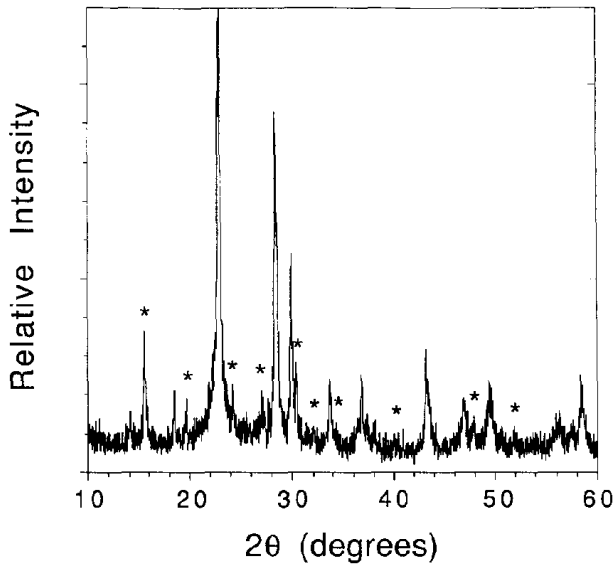

FIG. 9. X-ray powder diffraction pattern of a partially transformed aqueous-solvent-derived $VOHPO_4 \cdot 1/2H_2O$ powder, heated at 400°C for 2 hr in N_2, showing the coexistence of $VOHPO_4 \cdot 1/2H_2O$ (*) and $(VO)_2P_2O_7$.

diffraction patterns showing only a few broad, weak lines in this temperature region. The phase constitution during the course of the transformation may be dependent upon a number of different variables. While many literature reports (4, 9, 17, 18) mention the appearance of an amorphous intermediate, such an intermediate, devoid of any long-range order, is not required or suggested by the mechanism that is proposed here. A previous study (9) has noted that the nature of the transformed product is highly dependent upon the time, temperature, and atmosphere of heat treatment, as well as the properties of the precursor itself. In that study, the formation of an X-ray amorphous intermediate was observed, but the precursor used was derived from an organic synthesis medium and, thus, known to exhibit crystallographic disorder associated with its retained alcohol content (1, 9, 19). That precursor disorder is known (1, 9, 19) to result in an associated disorder in the pyrophosphate product and likely encourages the formation of a highly disordered (i.e., X-ray amorphous) intermediate. In the present study, where the transformation characteristics, in an inert atmosphere, of an aqueous medium derived precursor (with a correspondingly high level of crystallinity) have been studied, no obvious sign of an amorphous phase has been observed. In fact, in contrast to observations made by Amorós *et al.* (4), we note the simultaneous existence (as shown in Fig. 9) of vanadyl hydrogen phosphate and vanadyl pyrophosphate. Both are quite crystalline and occur in the absence of any amorphous intermediate.

While the total loss of periodicity is not required by the

mechanism presented here, some disorder in the pyrophosphate, particularly along the c axis, is predicted. As the individual crystallites form, the pyrophosphate groups may at first be disordered, randomly occupying positions above and below any given vanadium–oxygen "layer". Then, at higher temperatures, the P_2O_7 units rearrange, through inversion along the c direction, to lock into their energetically stable positions. Vanadium-atom double chains, composed of one chain with vanadyl (V=O) bonds all pointing along $+c$ and the other chain pointing along $-c$, may also be disordered relative to one another.

To assess the energetics associated with the transformation process, calculations were carried out. The mechansim of forming a pyrophosphate unit $[O_3P–O–PO_3]^{4-}$ from two tetrahedral $[O_3P–OH]^{2-}$ units in adjacent layers, depicted in Figs. 8b–8e, can be written as follows:

$$[O_3P–OH]^{2-} + [O_3P–OH]^{2-} \rightarrow [O_3P–O]^{3-} + [O_3P–OH_2]^{1-} \quad \Delta H_1 \quad [1]$$

$$[O_3P–OH_2]^{1-} \rightarrow [O_3P]^{1-} + OH_2 \quad \Delta H_2 \quad [2a]$$

$$[O_3P–O]^{3-} + [O_3P]^{1-} \rightarrow [O_3P–O–PO_3]^{4-} \quad \Delta H_3 \quad [2b]$$

$$[O_3P–O]^{3-} + [O_3P–OH_2]^{1-} \rightarrow [O_3P–O–PO_3]^{4-} + OH_2 \quad \Delta H_4 \quad [3]$$

First, within a layer, a proton transfer occurs from one $[O_3P–OH]^{2-}$ unit to another to form $[O_3P–O]^{3-}$ and $[O_3P–OH_2]^{1-}$ (Eq. [1]). Then, a pyrophosphate unit, $[O_3P–O–PO_3]^{4-}$, is formed between adjacent layers from the $[O_3P–O]^{3-}$ and $[O_3P–OH_2]^{1-}$ units. This may take either a two-step process (Eq. [2]), or a one-step process (Eq. [3]).

Estimates of the energetics involved in the reactions shown in Eqs. [1]–[3] were carried out using MNDO SCF-MO (20, 21) calculations on the basis of the isolated molecular systems generated by taking O^{2-} to be OH^-. For example, $[O_3P–OH]^{2-}$ is represented as $(HO)_3P–OH^+$. These calculations show that ΔH_1 = 182 kcal/mole, ΔH_2 = 45 kcal/mole, ΔH_3 = −148 kcal/mole, and ΔH_4 = −103 kcal/mole. The $[O_3P]^{1-}$ ion produced in Eq. [2a] is calculated to be planar, so the reactions of $[O_3P–O]^{3-}$ and $[O_3P]^{1-}$ (Eq. [2b]) should not encounter any activation energy. As a result, the two-step process (Eqs. [2a] and [2b]) requires an activation energy of about 45 kcal/mole. Our calculations of the reaction coordinates for the one-step process (Eq. [3]) show that the activation barrier of the reaction is about 40 kcal/mole, which is slightly smaller than, but comparable in magnitude to, the activation energy of the two-step process. Therefore, with this energy requirement, both the one- and two-step processes are likely to occur in the temperature region where conversion takes place (> ca. 375°C).

The transformation of the *cis* arrangement (Fig. 8c) of two adjacent vanadyl groups to the *trans* arrangement (Fig. 8d) requires the pyramidal inversion of one vanadium center. We estimate the activation barrier of this process by performing ZINDO (22, 23) calculations on an isolated model system composed of two octahedra sharing an edge, $(HO)_4VO_2V(OH)_4^{4-}$ (O shared between the two octahedra). The activation barrier for the conversion of the *cis* edge-shared arrangement to the *trans* edge-shared arrangement, and vice versa, is calculated to be about 36 kcal/mole.

For the temperature region where conversion of the precursor to pyrophosphate occurs, the inversion mechanism appears very reasonable, both structurally and energetically. According to the calculated enthalpies of the above reactions, the proton transfer step (Eq. [1]) requires the most energy. It is clear, however, that this proton transfer must occur during the structural transformation, regardless of the transformation mechanism, because two molecules of H_2O must be released from two $VOHPO_4 \cdot 1/2H_2O$ formula units: one water molecule that bridges the vanadium atoms, and one from the condensation of two $[O_3P–OH]^{2-}$ groups (Figs. 1 and 8). The pyramidal inversion of one phosphorus center and the conversion of *cis* to *trans* arrangement of adjacent vanadyl groups are energetically less demanding than the proton transfer step.

CONCLUDING REMARKS

A detailed study of the transformation from vanadyl hydrogen phosphate, $VOHPO_4 \cdot 1/2H_2O$, to vanadyl pyrophosphate, $(VO)_2P_2O_7$, was conducted at 500–700°C under nitrogen. Electron microscopy and X-ray diffraction clearly show the transformation to be topotactic: single crystals are converted to pseudomorphs which are unchanged in size or shape with respect to the starting crystals. Because the transformation of the precursor to the pyrophosphate is topotactic, the morphology of the precursor is, consequently, very important since it controls the morphology of the catalyst (24). Electron microscopy and X-ray and electron diffraction measurements show that the transformed pseudomorphs are made up of highly oriented microcrystals, and the orthorhombic unit cell axial directions essentially coincide with the unit cell axes of the starting orthorhombic, precursor, single crystal. To account for the above experimental observations, we have presented a detailed description of the transformation mechanism which involves phosphorus inversion.

A large contraction in the direction perpendicular to the basal plane, which accompanies the transformation process, induces cracks parallel to the basal plane and voids within the crystal thereby allowing the macroscopic thickness of the pseudomorph to remain unchanged. Diffraction results show that intercrystallite alignment is largely maintained in the basal plane, but a slightly greater degree of intercrystallite misalignment is inroduced along

the *c* axis. The generation of cracks to accommodate unit cell shrinkage along the thin dimension of the crystal plates creates additional basal plane surface area. The creation of this additional surface area may be beneficial in terms of catalytic performance. The design of precursor analogs with expanded basal plane spacings, which would result in larger unit cell shrinkages perpendicular to the basal plane and, presumably, the creation of yet more basal plane surface area via more extensive cracking, may lead to improved catalysts.

ACKNOWLEDGMENTS

The authors thank E. T. Jones and C. R. Miao for technical assistance, L. Lardear for precession camera work, W. J. Marshall for assistance with the single crystal X-ray diffractometer, C. M. Foris for X-ray powder diffraction patterns, J. F. Pedrick, E. Ervin, and K. Warrington for SEM work, J. Heitur for TEM work, C. Michel and B. Ruesswick for photographs, and L. Abrams for surface area measurements. We are also grateful to R. L. Harlow and Professor E. Bordes for helpful discussions and to P. D. VerNooy for providing the lattice parameters of $(VO)_2P_2O_7$ obtained from a blue, disorder-free single crystal. Work at North Carolina State University was supported by the Office of Basic Energy Sciences, Division of Materials Sciences, U. S. Department of Energy, under Grant DE-FG05-86ER45259.

REFERENCES

1. G. Busca, F. Cavani, G. Centi, and F. Trifiro, *J. Catal.* **90,** 400 (1986).
2. E. Bordes, P. Courtine, and J. W. Johnson, *J. Solid State Chem.* **55,** 270 (1984).
3. J. W. Johnson, D. C. Johnston, A. J. Jacobson, and J. F. Brody, *J. Am. Chem. Soc.* **106,** 8123 (1984).
4. P. Amorós, R. Ibáñez, A. Beltrán, D. Beltrán, A. Fuertes, P. Gomez-Romero, E. Hernandez, and J. Rodriguez-Carvajal, *Chem. Mater.* **3,** 407 (1991).
5. Yu. E. Gorbunova and S. A. Linde, *Sov. Phys.-Dokl. (Engl. Transl.)* **24,** 138 (1979).
6. C. C. Torardi and J. C. Calabrese, *Inorg. Chem.* **23,** 1308 (1984).
7. M. E. Leonowicz, J. W. Johnson, J. F. Brody, H. F. Shannon, Jr., and J. M. Newsam, *J. Solid State Chem.* **56,** 370 (1985).
8. P. D. VerNooy, to be published.
9. H. S. Horowitz, C. M. Blackstone, A. W. Sleight, and G. Teufer, *Appl. Catal.* **38,** 193 (1988).
10. G. Centi, F. Trifiro, and G. Poli, *Appl. Catal.* **19,** 225 (1985).
11. M. R. Thompson, A. C. Hess, J. B. Nicholas, J. C. White, J. Anchell, and J. R. Ebner, *in* "New Developments in Selective Oxidation II" (V. Cortés Corberán and S. Vic Bellón, Eds.), p. 167. Elsevier, Amsterdam/New York, 1994.
12. L. S. Dent Glasser, F. P. Glasser, and H. F. W. Taylor, *Q. Rev. (London)* **16,** 343 (1962).
13. S. Brunauer, P. H. Emmett, and E. Teller, *J. Am. Chem. Soc.* **60,** 309 (1938).
14. G. Busca, F. Trifiro, J. R. Ebner, and V. M. Franchetti, *Chem. Rev.* **88,** 55 (1988).
15. E. Bordes, *Catal. Today* **1,** 572 (1987).
16. K. Inumaru, T. Okuhara, and M. Misono, *Chem. Lett.* 1955 (1992).
17. J. B. Parise, H. S. Horowitz, T. Egami, W. Dmowski, and A. W. Sleight, *J. Catal.* **118,** 494 (1989).
18. G. A. Sola, B. T. Pierni, and J. O. Petunchi, *Catal. Today* **15,** 537 (1992).
19. G. Busca, G. Centi, and F. Trifiro, *J. Am. Chem. Soc.* **107,** 7757 (1985).
20. M. J. S. Dewar and W. Thiel, *J. Am. Chem. Soc.* **99,** 4899 (1977).
21. M. J. S. Dewar, M. L. McKee, and H. S. Rzepa, *J. Am. Chem. Soc.* **100,** 3607 (1978).
22. M. C. Zerner, G. H. Loew, R. F. Kirchner, and U. T. Mueller-Westerhoff, *J. Am. Chem. Soc.* **102,** 589 (1980).
23. W. P. Anderson, W. D. Edwards, and M. C. Zerner, *Inorg. Chem.* **25,** 2728 (1986).
24. E. Kesteman, M. Merzouki, B. Taouk, E. Bordes, and R. Contractor, "6th International Symposium on Scientific Bases for the Preparation of Heterogeneous Catalysts, Louvain-la-Neuve, Belgium, Sept. 5–8," p. 301, 1994.